Ab initio study of the relation between electric polarization and electric field gradients in ferroelectrics

J. N. Gonçalves,[1,*] A. Stroppa,[2] J. G. Correia,[3] T. Butz,[4] S. Picozzi,[2] A. S. Fenta,[1] and V. S. Amaral[1]

[1]*Departamento de Física and CICECO, Universidade de Aveiro, 3810-193 Aveiro, Portugal*

[2]*CNR-SPIN, 67100 L'Aquila, Italy*

[3]*Instituto Tecnológico e Nuclear, UFA, 2686-953 Sacavém, Portugal*

[4]*Fakultät für Physik und Geowissenschaften, Institut für Experimentelle Physik II, Universität Leipzig, Linnéstrasse 5, 04103 Leipzig, Germany*

(Received 27 February 2012; revised manuscript received 16 May 2012; published 26 July 2012)

The hyperfine interaction between the quadrupole moment of atomic nuclei and the electric field gradient (EFG) provides information on the electronic charge distribution close to a given atomic site. In ferroelectric materials, the loss of inversion symmetry of the electronic charge distribution is necessary for the appearance of the electric polarization. We present first-principles density functional theory calculations of ferroelectrics such as $BaTiO_3$, $KNbO_3$, $PbTiO_3$ and other oxides with perovskite structures, by focusing on both EFG tensors and polarization. We analyze the EFG tensor properties such as orientation and correlation between components and their relation with electric polarization. This work supports previous studies of ferroelectric materials where a relation between EFG tensors and polarization was observed, which may be exploited to study the ferroelectric order when standard techniques to measure polarization are not easily applied.

DOI: 10.1103/PhysRevB.86.035145 PACS number(s): 77.84.Bw, 77.22.Ej, 31.30.Gs

I. INTRODUCTION

There is great interest in ferroelectric/multiferroic materials nowadays due to their potential application in a plethora of subjects, ranging from high density memories to magnetoelectric sensors.[1–3] The complexity of electronic phenomena at the nanoscale makes them a hot research topic and a fertile ground for new experimental techniques, which are able to probe pointlike, atomic-scale properties. To this aim, the use of local probes as in hyperfine interactions techniques, such as Mössbauer effect spectroscopy, perturbed angular correlation (PAC) spectroscopy, nuclear magnetic resonance (NMR), and nuclear quadrupole resonance (NQR), give access to atomic scale information of the electronic charge density[4] through the measure of the electric field gradients (EFGs), thus probing the phenomenology of materials at the nanoscale.

From a theoretical point of view, advances in modern density functional theory have made the calculation of the spontaneous electric polarization P a routine calculation in an *ab initio* framework.[5–7] Recently, the calculation of EFGs has also become possible from first-principles.[8–14] However, to the best of our knowledge, a theoretical study based on *ab-initio* density functional methods aiming to investigate both the P and EFGs in a ferroelectric material is still missing in the current literature despite the fact that a linear correlation[15–17] between P and EFG values at a given site was shown a long time ago. This "correlation" would suggest that information obtained through the measurements of EFG tensors can provide indirect access to the polarization as well. If true, one could study a macroscopic property of the crystal, such as P by using local probes. In this work, we want to explore such a possibility.

A nucleus with a nonspherical nuclear charge distribution possesses an electric quadrupole moment which leads to a hyperfine splitting for a nuclear spin $I \geqslant 1$ if subjected to an EFG. The hyperfine techniques previously mentioned can measure the quadrupole coupling constant, which is the interaction between the nuclear quadrupole moment and the EFG. The EFG, in turn, arises due to the Coulomb potential at the nucleus, and its measurement is sensitive to the surrounding electronic charge density. More precisely, it is defined as the symmetric traceless second-rank tensor of second derivatives of the Coulomb potential with respect to the spatial coordinates, $V_{ij} = \partial^2 V/(\partial x_i \partial x_j)$, at the nuclear position. In the principal axis coordinate system, the tensor is diagonal and its elements are usually ordered by the convention $|V_{zz}| \geqslant |V_{yy}| \geqslant |V_{xx}|$. Usually V_{zz} and the asymmetry parameter $\eta = (V_{xx} - V_{yy})/V_{zz}$ are used in the analysis of measurements. We recall that the EFG is site dependent, and its principal axes $(\tilde{x},\tilde{y},\tilde{z})$ may not be the same at every site, although they are usually along symmetry axes of the crystal. EFG studies are found in various types of materials, for example, intermetallics,[18] metal complexes,[19] magnetic,[20] or multiferroic compounds.[21]

Previous studies have shown that in some ferroelectric materials P follows a temperature dependence which can be related to the EFG at specific atomic sites. For instance, NMR using ^{23}Na in Rochelle salts $[NaK(tartrate)\cdot 4H_2O]$ showed that P and the EFG are linearly related.[15–17] In 1978 Yeshurun suggested[22] that the EFG due to static displacements should be proportional to P^2 in perovskite crystals using an empirical model for interpreting previous ^{57}Fe Mössbauer measurements in $BaTiO_3$.[23] Dynamical aspects were also considered by relating the EFG to the electric susceptibility, and it was found that the EFG should have a critical behavior when approaching T_C.[22] This peculiar feature was recently used in the identification of ferroelectricity with EFG measurements.[24] In this work, $Pr_{1-x}Ca_xMnO_3$ was studied with the measurement of the EFG at ^{111m}Cd probes implanted into the sample. An abrupt change was found in a short temperature interval. This was associated to the onset of ferroelectricity, since the EFG should

be dominated by a contribution proportional to the electric susceptibility at the transition, i.e., with its critical behavior.[22] In the same work,[24] it was also suggested that the temperature dependence of EFG tensors can give information on the onset of charge or orbital ordering. In Ref. 25 it was argued that the static part of V_{zz} should have the following behavior with respect to P: either it is proportional to P^2 in sites which have inversion symmetry in the paraelectric structure, or it is proportional to P, like in Rochelle salts. The quadratic relation was supported by experiments in $NaNO_2$,[25] in $PbHfO_3$ not too close to T_C (where critical behavior is found), by PAC measurements,[4,26] and by NMR measurements in $BaTiO_3$.[27] It is therefore clear from the current literature that P and the EFG tensor are closely related quantities.

Our study aims to explore this relationship by calculating both P and EFG for simple ferroelectric materials and studying a possible correlation between these quantities. Some of the previously mentioned results are obtained by impurity probes in the host materials. Here, we shall limit our studies to systems where the probes are natural constituents of the materials.

This work is organized as follows. In Sec. II we discuss the computational details. In Sec. III A we present the results and discuss the relationship between P and EFGs for simple tetragonal or orthorhombic (Sec. III B) systems. We analyze the possible linear correlations between EFG tensor components in Sec. III C. A study of the variation of $V_{zz}(P)$ with the atomic numbers of different materials is shown in Sec. IV. Finally, in Sec. V we draw our conclusions.

II. TECHNICAL DETAILS

We have considered a series of simple ABO_3-type perovskite compounds.[28] For $BaTiO_3$, $PbTiO_3$, and $KNbO_3$ we have considered the tetragonal experimental structures as references. We also considered other perovskite-related compounds, such as $BaZrO_3$, $CaTiO_3$, $PbZrO_3$, $SrTiO_3$, $NaNbO_3$, and $LiNbO_3$ by considering a pseudocubic phase at the experimental lattice constants of the cubic paraelectric phase. The ferroelectric distortion was mimicked by a polar displacement of the atoms. The experimental displacements in tetragonal $BaTiO_3$ are $z_{Ti} = 0.0203$, $z_{O1} = -0.0258$, and $z_{O2} = -0.0123$, in fractional coordinates.[29] We calculate the EFG as a function of λ, which represents the fraction of the displacements (z_{Ti}, z_{O1}, z_{O2}) mentioned above. Therefore $\lambda = 1$ corresponds to the equilibrium (experimental) structure. Values of $0 \leqslant \lambda \leqslant 1.2$ are used, i.e., $\lambda = 0$ corresponds to undistorted, $\lambda = 1$ corresponds to the experimental equilibrium distortion (at 280 K), and $\lambda = 1.2$ corresponds to 20% additional distortion. For the compounds where the cubic structure is used, a ferroelectric state is considered using the same fractional distortions as in $BaTiO_3$. Although these states may not be observed in normal conditions, this allows us to study the possible correlation of polarization and EFG in different systems or as a function of strain.

For the density functional theory calculations we used the projector-augmented-wave (PAW) method,[30] as implemented in the *Vienna ab-initio simulation package* (VASP),[31] with the generalized gradient approximation (GGA)–Perdew, Burke, and Ernzerhof (PBE) functional.[32] We used a Γ-centered Monkhorst-Pack $7 \times 7 \times 7$ k-points grid, and an energy cutoff of 400 eV. The polarization is calculated with the Berry phase approach.[6,7] The EFG is calculated at the atomic sites A, B, apical O1, and equatorial O2 sites.

TABLE I. Lattice constants (in Å) and atomic distortions used in the calculations of the perovskite compounds. δ_A, δ_B, δ_{O1}, δ_{O2} correspond to the fractional distortions in the c direction, with respect to the ideal positions, of the inequivalent sites. Sites A are at the corners of the unit cell, B is the transition metal inside an octahedron formed by apical O1 and equatorial O2 oxygen atoms.

Compound	a	c	δ_A	δ_B	δ_{O1}	δ_{O2}
$BaTiO_3$[a]	4.00	4.03		0.02	−0.03	−0.01
$KNbO_3$[b,c]	4.00	4.06	0.02		0.04	0.04
$PbTiO_3$[d,e]	3.90	4.16		0.04	0.11	0.12
$BaZrO_3$[f]	4.19					
$CaTiO_3$[f]	3.83					
$NaNbO_3$[f]	3.94					
$PbZrO_3$[f]	4.13					
$SrTiO_3$[f]	3.91					
$LiNbO_3$[g]	4.00					

[a]Reference 29.
[b]Reference 34.
[c]Reference 35.
[d]Reference 36.
[e]Reference 37.
[f]Cubic lattices, experimental values (Ref. 28).
[g]Theoretical lattice parameter, found by the volume optimization in the cubic phase, with atoms at the ideal positions.

For the case of $BaTiO_3$ we also performed calculations with the L/APW + lo method, implemented in the WIEN2K code.[33] The basis set was limited by $RK_{max} = 8$, where RK_{max} stands for the product of the smallest atomic sphere radius R_{mt} times the largest K-vector K_{max} of the plane wave expansion of the wave function, and a $6 \times 6 \times 6$ k-points grid was used.

III. RESULTS AND DISCUSSION

A. Relation between EFGs and P

The lattice constants are shown in Table I, along with the experimental atomic distortions in the ferroelectric compounds $BaTiO_3$, $KNbO_3$, and $PbTiO_3$. For the other cases, we have considered the fractional distortion of $BaTiO_3$.

Let us start by considering the case of $BaTiO_3$. The variation of the total energy with the atomic distortions is shown in Fig. 1(a), with the displacements considered along the polar axis z in both directions. The curve shows the expected double well profile. The energy minimum is reached for 85% of the experimental distortion: the slight discrepancy is probably due to the approximation used here for the exchange-correlation functional. Given that both the experimental/theoretical displacements are very small, this discrepancy is reasonable.[38] In all the following cases, the vertical dashed and dotted lines correspond to the theoretical energy minimum and the experimental distortions, respectively. The stable state has an energy lower than the undistorted one by 20 meV, which compares well with previous calculations.

Figure 1(b) presents P as a function of the ferroelectric distortion. It can be seen that P is approximately a linear

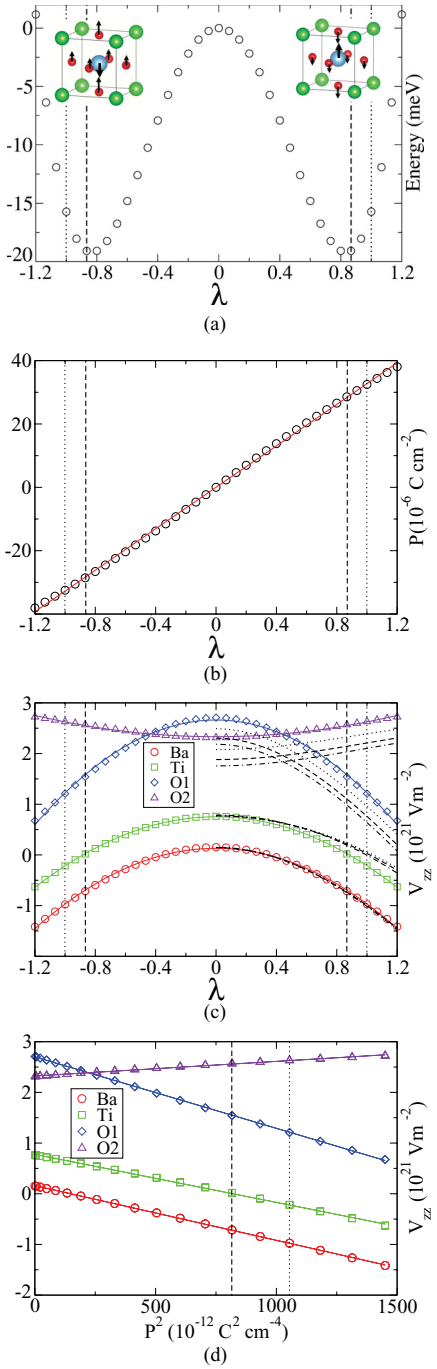

FIG. 1. (Color online) $BaTiO_3$ in the tetragonal phase. (a) Energy (meV) as a function of distortion, varied in equal intervals from 0 to 1.2. The direction of the displacements is shown at each side in the plot. (b) P (μC cm^{-2}) as a function of distortion. The vertical dashed and dotted lines correspond to the calculated energy minimum and experimental distortion, respectively. (c) V_{zz} (10^{21} V m^{-2}) as a function of distortion (dotted, dashed, and dot-dashed lines are L/APW + lo calculations; see text). (d) V_{zz} as a function of P^2 (10^{-12} C^2 cm^{-4}). Full lines are fits to the data.

function of the distortion. This is not unexpected since we are considering displacive-type ferroelectrics, as already discussed in previous works.[39] The calculated P at the experimental distortions is 28.6 μC cm^{-2}, according to what can be seen in Fig. 1(b), while the experimental one[40] is 27 μC cm^{-2}.

In Fig. 1(c) we show the EFG component V_{zz} as a function of distortion for all sites.[41] It is evident that V_{zz} shows a quadratic dependence upon the distortion. The sign[42] and magnitude of the values obtained are consistent with previous calculations.[42,43] Measurements[44] obtained at the O sites by NMR are in agreement for the equatorial site with 2.56, but at the apical site the experimental value is 2.06, while our calculated value is smaller, 1.2 (all in units of 10^{21} V m^{-2}).

Furthermore, we investigated how the EFG results depend on the choice of method or functional [see Fig. 1(c)]. We have performed calculations using the L/APW + lo implementation of DFT, with the WIEN2K code. Three different functionals were used, which are represented in the plot by dotted, dashed, and dot-dashed lines, corresponding to the GGA-PBE,[32] GGA–Wu and Cohen (WC),[45] and local-density approximation (LDA)[46] exchange-correlation functionals. The variation of EFG with distortion is the same, except for a small difference at Ti between the two implementations. There is also a shift in values at the O atoms, with a maximum difference of 0.5×10^{21} V m^{-2}, when comparing LDA L/APW + lo and PBE PAW calculations, while maintaining the same variation with distortion. These differences are reasonable and the main feature, quadratic variation of V_{zz} with distortion, remains the same. All the following results are taken from the PAW calculations.

In order to get rid of the distortion parameter, in Fig. 1(d) we plot the V_{zz} EFG component as a function of P^2. In this case, a fit of the data clearly shows a linear dependence.

For $KNbO_3$ the trends are similar, and a linear relation is also obtained in Fig. 2(a). In this case, the calculated value of P at the experimental distortion is 37.4 μC cm^{-2},

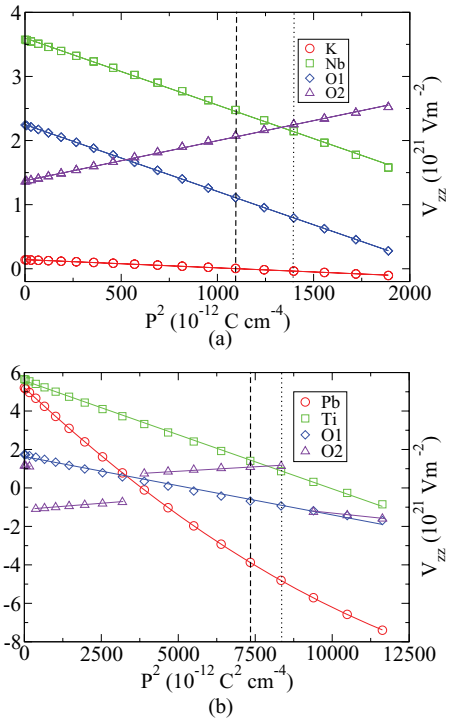

FIG. 2. (Color online) V_{zz} at each site as a function of P^2 (10^{-12} C^2 cm^{-4}). The lines are fits to the $V_{zz}(P^2)$ data. (a) $KNbO_3$, (b) $PbTiO_3$, in the tetragonal phases.

TABLE II. Coefficients a for the fits of the expression $V_{zz}(P) = V_{zz}^0 + a \times P^2$. V_{zz}^0 in units of 10^{21} V m^{-2}, a in units of 10^{22} V C^{-2} m^2, for the compounds with tetragonal- and cubic-perovskite-type structures.

	$BaTiO_3$		$KNbO_3$		$PbTiO_3$		$BaZrO_3$		$CaTiO_3$		$PbZrO_3$		$SrTiO_3$		$NaNbO_3$		$LiNbO_3$	
	V_{zz}^0	a	V_{zz}^0	a	V_{zz}^0	a	V_{zz}^0	a	V_{zz}^0	a	V_{zz}^0	a	V_{zz}^0	a	V_{zz}^0	a	V_{zz}^0	a
A	0.16	−1.079	0.14	−0.128	5.28	−1.787[a]	0.00	−0.945	0.00	−0.186	−0.01	−1.911	0.00	−0.551	0.00	−0.077	0.00	−0.012
B	0.78	−0.949	3.60	−1.046	5.58	−0.562	0.00	−0.757	0.01	−0.724	−0.02	−0.985	0.01	−0.834	0.00	−0.163	0.00	−0.311
O1	2.70	−1.410	2.25	−1.042	1.63	−0.303	−1.43	−1.124	−0.11	−1.025	−3.61	−1.009	1.08	−1.193	0.30	−0.882	0.67	−0.940
O2	2.32	0.288	1.37	0.625	1.18	−0.461[b]	−1.41	0.300	−0.10	0.349[c]	−3.59	0.232	1.11	0.253	0.32	0.389	0.69	0.363

[a]An additional quartic term $b \times P^4$, with $b = 3.626 \times 10^{21}$ V C^{-4} m^6, is needed to get a satisfactory fit for this atom.
[b]This coefficient fits a component that is V_{zz} in the paraelectric phase, but is interchanged with other components in the distortion path. An additional quartic term $b \times P^4$, with $b = 1.157 \times 10^{21}$ V C^{-4} m^6, is needed to get a satisfactory fit for this atom.
[c]This coefficient fits a component that is V_{zz} in the paraelectric phase, but is interchanged with with other components in the distortion path. An additional quartic term $b \times P^4$, with $b = -4.643 \times 10^{21}$ V C^{-4} m^6, is needed to get a satisfactory fit for this atom.

consistent with the measured value.[39] The calculated V_{zz} at Nb, 2.6×10^{21} V m^{-2} is also consistent with $|V_{zz}| = 2.7 \times 10^{21}$ V m^{-2} obtained by an NMR experiment at 220 C (Ref. 47) [considering $Q_{^{93}\mathrm{Nb}} = -0.37b$ (Ref. 48)].

For the case of $PbTiO_3$, presented in Fig. 2(b), much larger values of polarization are obtained. The polarization is 85 (91) at the calculated (experimental) distortion, higher than the measured[34] 75 μC cm^{-2} at room temperature. Notably large variations of the EFG in the range of distortions are seen at the Pb and Ti sites. The obtained values of V_{zz} are in reasonable agreement with Ti NMR experiments (Table III of Ref. 49) (better agreement is seen considering the calculation of minimum energy). V_{zz} at the O2 site has discontinuous changes, but the EFG tensor is continuous, as will be shown later.

The coefficients in the $V_{zz}(P)$ expression obtained are shown in Table II, for all the atoms in the unit cell of all compounds considered. At the A, B, and apical O1 atoms, the relation found in almost all the compounds considered here is $\begin{pmatrix} \Delta V_{xx} & 0 & 0 \\ 0 & \Delta V_{yy} & 0 \\ 0 & 0 & \Delta V_{zz} \end{pmatrix} = \Delta P^2 \times \begin{pmatrix} a_{xx} & 0 & 0 \\ 0 & a_{yy} & 0 \\ 0 & 0 & a_{zz} \end{pmatrix}$. However, since these sites have $\eta = 0$, the tensor is defined by only one independent parameter. $V_{xx} = V_{yy} = -1/2V_{zz}$, and the quadratic coefficients also follow the same symmetry $a_{xx} = a_{yy} = -1/2a_{zz}$. The equatorial oxygen sites (O2) do not have an n-fold rotation axis with $n \geqslant 3$. This implies that the asymmetry parameter is not zero. In this case the coefficients of P^2 describing the variation of the EFG tensor do not show such a simple relation.

The variation of the EFG with displacements can be understood by considering a Taylor series expansion,

$$V_{zz} = V_{zz}^0 + \sum_i \frac{\partial V_{zz}}{\partial r_i} \delta r_i + \sum_i \frac{\partial^2 V_{zz}}{\partial r_i^2} \delta r_i^2 + \cdots,$$

where δr_i are small deviations of the atomic positions relative to the paraelectric structure. When the transition involves small displacements and for atoms where the EFG does not undergo large changes in the transition this expansion should converge rapidly. For sites without inversion symmetry, the linear term should be dominant, whereas for sites with inversion symmetry the linear term vanishes and the quadratic term in the expansion becomes relevant.[25]

The V_{zz} component follows a quadratic variation for all the atoms in all the compounds studied, with only two exceptions, $PbTiO_3$ and $CaTiO_3$. At the O2 sites of $PbTiO_3$ and $CaTiO_3$ there are interchanges of tensor components which make the description of EFG variations in terms of the V_{zz} component inadequate. At the Pb site of $PbTiO_3$ a small quartic term in the polarization is found necessary for a good fit of $V_{zz}(P)$ ($a \times P^2 + b \times P^4$) (terms with odd powers of P are not allowed due to the inversion symmetry, in the paraelectric structure, of the sites involved in the distortion).

In the paraelectric structure of $BaTiO_3$ the principal component of the tensor V_{zz} for Ba and Ti is directed along the z axis. For the O atoms, the EFG tensor is also aligned with the tetragonal crystalline axes, and V_{zz} is directed to the neighboring Ti atoms. For $BaTiO_3$, with increasing ferroelectric distortion (P), in all distortions calculated, the direction of V_{zz} remains the same for all atoms. The V_{xx} and V_{yy} components also maintain their directions in this path, for the Ba, Ti, and O1 atoms, along the x and y axes, respectively. For the O2 atoms, however, V_{xx} and V_{yy} do not always correspond to the same orientations. The three components of the EFG tensor for the O2 site in $BaTiO_3$ are shown in Fig. 3(a). At a given distortion, due to the convention $|V_{yy}| \geqslant |V_{xx}|$, the regular curves followed by these components are interchanged. For distortion $\lambda \leqslant 0.9$ the directions for V_{xx}, V_{yy} are z and x for O2 at (0.5,0,0.5), z and y for O2 at (0,0.5,0.5). For higher λ these directions are interchanged. Nevertheless, the quadratic behavior of EFG(P) is maintained here and this interchange is ignored. Table III shows the coefficients of the quadratic terms for the variation of the EFG tensor components at each crystalline axis direction in $BaTiO_3$. Unlike in the case of $\eta = 0$, the quadratic coefficients a do not have the same symmetry as the EFG tensor components.

The tensor component interchanges may only happen at the O2 sites, where η changes. For $BaZrO_3$, $PbZrO_3$, $NaNbO_3$, $LiNbO_3$, and $SrTiO_3$ there are no interchanges between tensor components, for $KNbO_3$ there is an interchange between V_{xx} and V_{yy}, while for $CaTiO_3$ and $PbTiO_3$ there are exchanges between the three components. For the sake of brevity, we only show here the O2 EFG tensor components for $PbTiO_3$ [Fig. 3(b)], where there are as many as five interchanges of one tensor component in the range of distortions considered. In particular, there is an interchange near the experimental distortion of which one should be aware in EFG

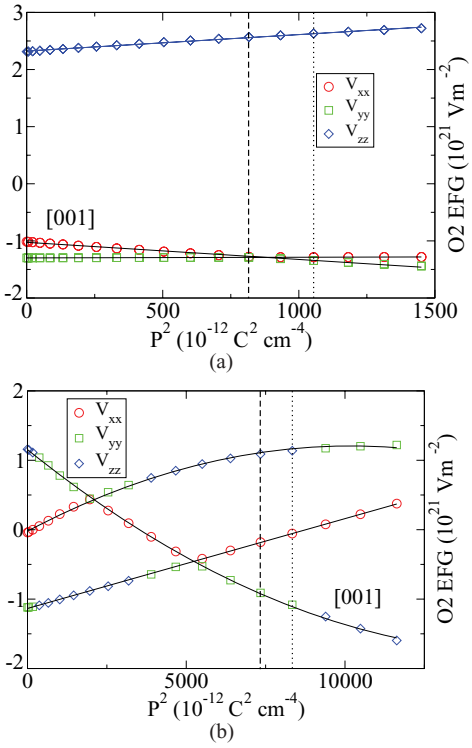

FIG. 3. (Color online) (a) $BaTiO_3$ in the tetragonal phase: V_{zz}, V_{yy}, and V_{xx} components of the EFG tensor for the O2 atoms as a function of P^2. The lines are fits to the tensor components with regular variation. (b) $PbTiO_3$ in the tetragonal phase: V_{zz}, V_{yy}, and V_{xx} components of the EFG for the O2 atoms as a function of P^2. The [001] direction curves are also indicated. Depending on the specific atom, the other two curves correspond to either the [100] or [010] directions.

measurements, since a kink measured in a V_{zz} dependence could be a consequence of the convention that V_{zz} is the largest EFG component in magnitude, instead of a phase transition.

Moreover, as already mentioned, to obtain a satisfactory fit to $V_{zz}(P)$ at the Pb site a small quartic term should also be considered [Fig. 2(b)]. $V_{zz}(P)$ follows approximately a linear behavior for larger values of P^2. At the O2 site two of the curves of components with constant direction also need quartic terms for a good fit [Fig. 3(b)]. The much larger displacements in this compound would indeed indicate that the $V_{zz}(\delta r)$ expansion does not converge as fast as in other cases. In order to confirm that with larger displacements additional terms must be included in $V_{zz}(P)$, we performed the calculation of $BaTiO_3$ again, but this time we doubled the size of the distortions, allowing $0 \leqslant \lambda \leqslant 2.4$. The variation of the EFG ceases to be properly described by a single quadratic term at the O sites, and an additional term is needed, as expected.

For the other cases there is only an exception in the O2 sites of $CaTiO_3$ where a quartic term is also needed. We point out that $CaTiO_3$ has the smaller unit cell (Table I), so the ions will be closer with the same λ in comparison to the other compounds, which may be related to this exception.

In the pseudocubic cases the chosen distortions are arbitrary. Nonetheless, we can conclude from these cases that, for small distortions, a simple quadratic variation of V_{zz} with polarization is seen in several different systems, apart from small deviations.

TABLE III. Fit coefficients for the O2 atoms. $V(P) = V^0 + a \times P^2$. V^0 in units of 10^{21} V m^{-2}, a in units of 10^{22} V m^{-2} C^{-2}.

Compound	EFG component	V^0	a
$BaTiO_3$	V_1	−1.31	0.019
	V_2	−1.03	−0.297
	V_3	2.32	0.288

B. Orthorhombic structure

$BaTiO_3$ exhibits monoclinic, rombohedral, and orthorhombic phases at different temperatures. In order to see what are the differences in the EFG and P with a change of structure, we have made a series of calculations in the orthorhombic phase. We also took one experimental measurement[29] of the orthorhombic structure as the reference distortion ($\lambda = 1$) and calculated from $\lambda = 0$ to $\lambda = 1.2$ of this distortion keeping the lattice parameters (a, b, c) constant. The theoretical distortion of minimum energy is once again found to be close to 85% of the experimental distortion.

The resolved components of the EFG tensors at the four inequivalent atoms against P^2 are displayed in Fig. 4, and the coefficients resulting from the fits are listed in Table IV. In this structure there is not a single site with axial symmetry, and the relationship between EFG and P will never be as simple as discussed above. There are also discontinuities in V_{zz} at Ba and Ti sites due to the interchange of components. Nevertheless, ignoring these interchanges, the relation for each direction is purely quadratic in all cases. These results, like the previous ones, show that there is no physical meaning in the change of the principal axis definition (as xx, yy, or zz), and that the conventional assignment may obscure a simpler relation with crystal axes.

C. Correlations between EFG tensor components

For the cases studied with tetragonal and cubic lattice parameters, $\eta \neq 0$ only for the O2 atoms. For $\eta = 0$ the components of the EFG are trivially related, but when $\eta \neq 0$, the possible correlation between tensor parameters should be studied. The usual parametrization of V_{zz} and η assumes uncorrelated EFG components. Instead, correlations between the components of the tensors may be studied in a plot of one component against the other. However, just plotting V_{zz} against V_{xx} results in a distorted cobweb plot, and EFG tensor trajectories obtained by continuous variation of some parameter (temperature, distortion, pressure) may not be continuous (when $\eta = 1$, V_{zz} changes sign). Czjzek proposed a different system to eliminate these problems,[50] initially to deal with the analysis of amorphous systems. However, it is also suited to investigate the correlations between the tensor components.[51,52] This plot uses $-2V_{xx}$ as a function of $|2(2V_{zz} + V_{xx})/\sqrt{3}|$. With this linear combination of tensor components, the trajectories are always continuous, and are straight lines if there is a linear dependence of V_{zz} on V_{xx}.

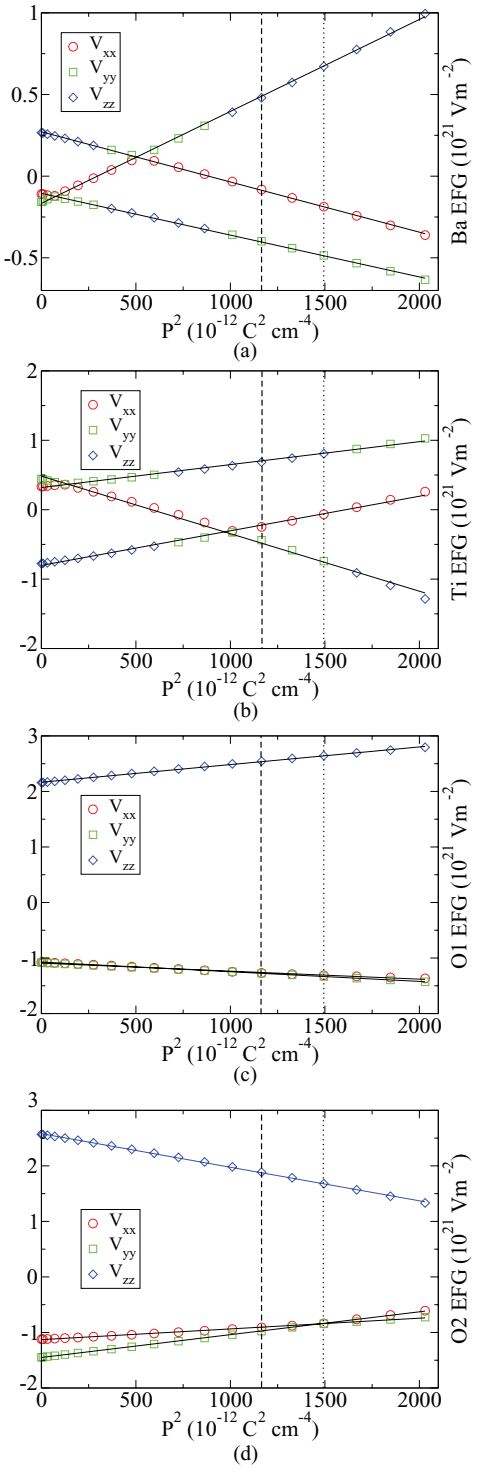

FIG. 4. (Color online) EFG tensor components in the principal coordinate system, of (a) Ba, (b) Ti, (c) O1, and (d) O2, as a function of P^2 for orthorhombic $BaTiO_3$. The lines are fits to the tensor components of regular variation.

The trajectories in the Czjzek plot of all the tetragonal cases are shown in Fig. 5 for the equatorial oxygen atoms, where η changes and a nontrivial correlation may be present. In this plot, the lines of constant η are the lines emerging from the origin: the boundary lines correspond to $\eta = 0$ and the horizontal line corresponds to $\eta = 1$. The herringbone

TABLE IV. Coefficients a for the fits of the expression $V(P) = V^0 + a \times P^2$ for $BaTiO_3$ in the orthorhombic phase, where $V_{1,2,3}$ is a component of the tensor with regular variation. $V_{1,2,3}$ in units of 10^{21} V m^{-2}, $a_{1,2,3}$ in units of 10^{22} V C^{-2} m^2.

	Ba	Ti	O1	O2
V_1^0	−0.17	−0.80	2.17	−1.13
a_1	0.563	0.498	0.318	0.193
V_2^0	−0.11	0.48	−1.07	−1.45
a_2	−0.256	−0.829	−0.174	0.411
V_3^0	0.27	0.32	−1.09	2.58
a_3	−0.307	0.331	−0.144	−0.605

lines correspond to constant V_{zz}. Reflections at the boundary of the plots, seen, for example, in $BaTiO_3$ and $KNbO_3$, are associated with the interchange of V_{xx} and V_{yy} components previously shown, and the crossing of the trajectory of the line $\eta = 1$ corresponds to a change in sign and orientation

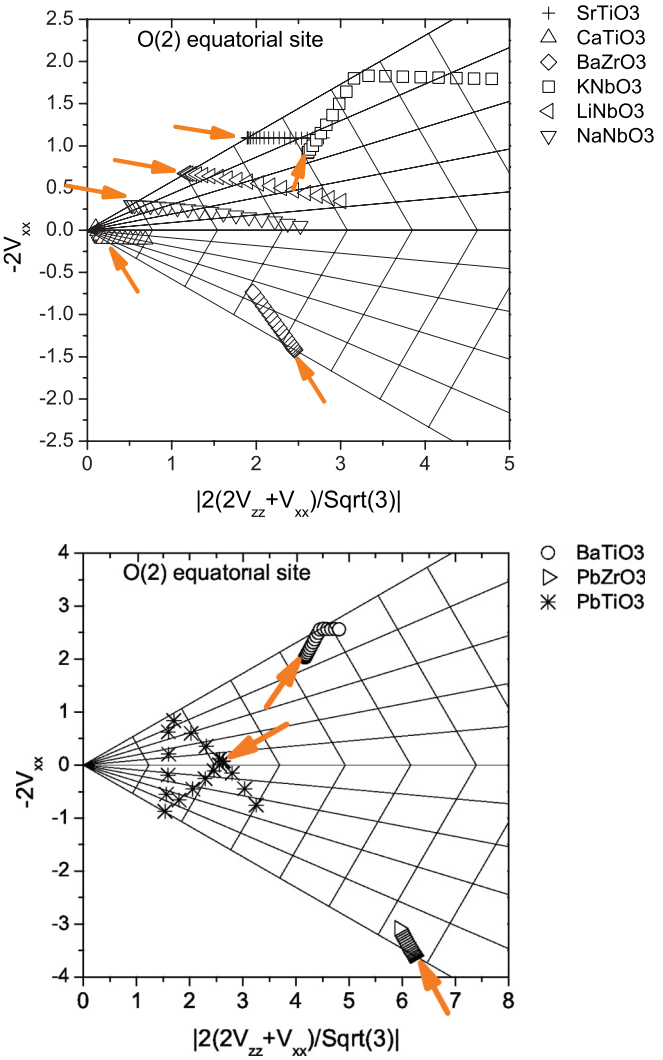

FIG. 5. (Color online) Cjzjek plots of the EFG tensor components at the equatorial O2 sites with P (or distortion) as the implicit parameter in the perovskite materials studied, covering $0 < \lambda < 1.2$, in units of 10^{21} V m^{-2}. The arrows indicate the "initial" point and direction of the trajectories, corresponding to $P = 0$. Trajectories start at $\eta = 0$ except for the tetragonal cases.

TABLE V. Approximate values for the lengths of the EFG(O2) trajectories in the Cjzjek plots, relative to the length of $BaTiO_3$, and their asymptotic asymmetry parameter (η_∞).

Compound	length	η_∞
$BaTiO_3$	1	0.92
$SrTiO_3$	0.99	1
$CaTiO_3$	0.85	1
$BaZrO_3$	0.88	0.81
$LiNbO_3$	1.91	0.63
$NaNbO_3$	2.02	0.77
$PbZrO_3$	0.59	0.92
$KNbO_3$	2.87	1
$PbTiO_3$	5.76	0.46

of V_{zz}. The equatorial oxygen sites still have axial symmetry ($\eta = 0$) in the paraelectric structure in the cubic structures, since there is fourfold rotation symmetry around the axes connecting the O to the B sites. Therefore, in these cases, the trajectories start at the boundary of the plot. For the tetragonal cases, this symmetry is lost and $\eta \neq 0$ even in the paraelectric phase: $\eta = 0.12$ for $BaTiO_3$, $\eta = 0.33$ for $KNbO_3$, and $\eta = 0.93$ for $PbTiO_3$. The upper (lower) wedge is for positive (negative) V_{zz}. The values of V_{zz}(O2) change significantly for the different compounds, even changing sign. $KNbO_3$, $SrTiO_3$, $LiNbO_3$, and $NaNbO_3$ always have positive values of V_{zz}, while the zirconates $BaZrO_3$ and $PbZrO_3$ have negative values of V_{zz} in distortions considered. The EFG changes sign in the trajectories of $CaTiO_3$ and $PbTiO_3$. In the case of $CaTiO_3$ the trajectory overlaps with itself. It starts at negative EFG and $\eta = 0$, then it goes to positive EFGs, in the direction of the arrow, it is reflected and comes back the same way, changing sign again, and finally it is reflected to the horizontal path. In general the positive EFGs increase in absolute value with distortion, while the negative ones decrease. Exceptions in this respect are parts of the trajectories in $PbTiO_3$ and $CaTiO_3$.

The lengths of the trajectories in this plot are presented in Table V. The lengths are markedly larger for $PbTiO_3$, $KNbO_3$, $LiNbO_3$, and $NaNbO_3$. The cases of $PbTiO_3$ and $KNbO_3$ correspond to different fractional distortions in comparison to the other cases. However, all the other cases have fractional distortions equal to $BaTiO_3$. In this respect, it is interesting to remark that both niobates ($LiNbO_3$ and $NaNbO_3$) have trajectories with approximately twice the length of the others, indicating that the local charge at the O2 atoms is more sensitive to displacements when Nb is the B site.

From these plots it is also of interest to determine the "asymptotic" asymmetry parameter (η_∞),[52] related to the slope of the trajectories after reflections at the boundaries, corresponding to the limiting value of η for a given trajectory. These values are presented in Table V. It can be seen that η_∞ is large in most cases, with a smaller value for $PbTiO_3$. It should be related to the different features of the distortion, due to the fact that this compound has ferroelectricity driven by the lone pair of s electrons at the Pb ions, while ferroelectricity in other compounds is related to the d^0 configuration at the B site.

If the trajectories in this plot are straight lines, this shows that the EFG tensor components are linearly related. This is usually the case, except for $LiNbO_3$ and $NaNbO_3$, where the trajectory is approximately straight for low values of P, but becomes curved for higher values. The linearity in almost all cases means that the whole tensor, when considering the distortions that give rise to ferroelectric polarization, can be described by a *single* parameter. This might have important implications on the way experimental data should be analyzed, since the components are not independent, and the combination of all information will be more useful than each of them taken separately. The study of the EFG dependence on temperature (or on other variables), usually done by separating V_{zz} and η, can be performed by identifying the global single parameter.

IV. RELATION BETWEEN EFG AND P IN DIFFERENT MATERIALS

In the following we analyze the relations found in different materials. The quadratic coefficients a in the $V_{zz}(P)$ expression follow an interesting trend with atomic number at the A sites (Z_A), shown in Fig. 6. Figures 6(a) and 6(b) show V_{zz} at the A site for the different cubic and tetragonal compounds. $PbTiO_3$ introduces larger variations for P^2 and V_{zz} which may follow from the larger displacements in the experimental distortion, related, as previously discussed, to the different nature of the ferroelectricity.

V_{zz} is 0 for the paraelectric cubic cases, while for the paraelectric tetragonal structures V_{zz}^A has small nonzero values, except $PbTiO_3$. The slopes of the trajectories correspond to the coefficients of the quadratic term, which are shown in Fig. 6(c). The A sites with a larger number of electrons show a larger magnitude of a, that follows a quadratic dependence on Z_A. There are two pairs of compounds with the same Z_A, but different metal B sites, namely $BaTiO_3$/$BaZrO_3$ and $PbTiO_3$/$PbZrO_3$. The same trend is still qualitatively followed although small changes in the values of the coefficient are seen, and the changes do not follow a pattern: a is higher for $B =$ Ti than $B =$ Pb in the cases with $A =$ Ba, but the opposite happens when $A =$ Pb. We did not find other trends for the other coefficients, or for V_{zz}^0, as a function of the atomic number of the different sites.

V. CONCLUSIONS

In summary, our calculations provide an *ab-initio* support for previous observations of a quadratic dependence of the EFG tensor versus P in ferroelectric materials with the perovskite structure and other distorted structures. An exception to this rule is only seen in $PbTiO_3$, at the Pb and equatorial O sites, and in $CaTiO_3$ at the equatorial sites, where an additional quartic term dependence is observed. Moreover, for most cases the local symmetry of the atom means that the EFG tensor is axially symmetric and all the components are trivially related to each other. For the equatorial oxygen atoms this is not the case. Nevertheless, the components of the EFG tensor are also quadratically related to P and there is a linear correlation among EFG tensor components for most cases. The relation between P and EFGs follows a trend with the atomic number of the A site, qualitatively a quadratic variation.

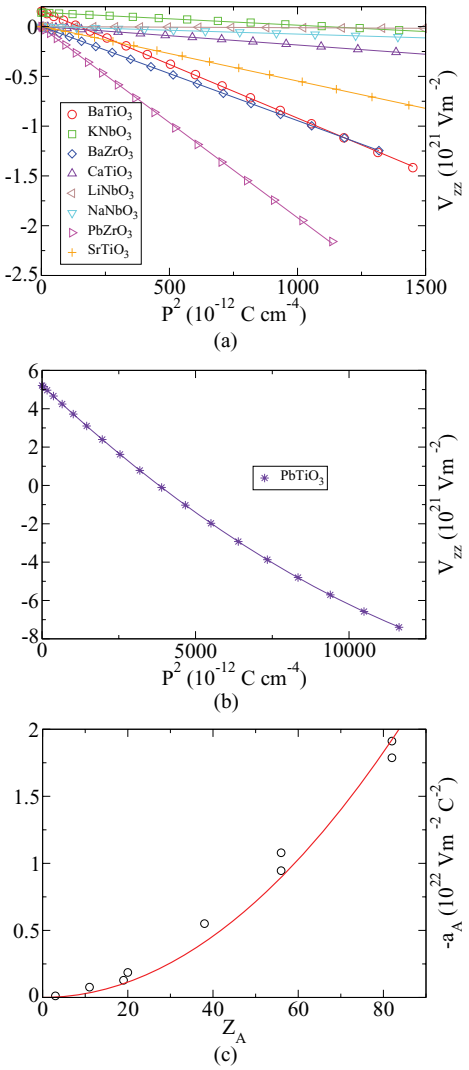

FIG. 6. (Color online) (a) V_{zz} at the A site as a function of P^2, showing the different coefficients (slopes of straight lines). (b) V_{zz} as a function of P^2 for $PbTiO_3$. (c) Coefficients of quadratic term of $V_{zz}(P)$, at the A site, for a series of materials with the perovskite structure, as a function of atomic number Z_A. The line is a quadratic fit.

The EFG, working as a local analog of P, has the added advantage of higher spatial resolution and short time scales, which allows local probing of nanoscale phenomena at specific lattice sites. The different types of lattice sites, including defects, can be discriminated by their different EFGs. Its critical behavior in phase transitions may be analyzed, and the order of the transitions can be established with a high degree of detail. In hysteresis loops, it can act as a static measurement of the electric polarization in individual domains, not limited by depolarization effects, and is much more sensitive to polarization reversal. It is also suited to probe phase coexistence or inhomogeneous polarization states with atomic selectivity, well beyond the reach of conventional polarization measurements. Moreover, piezoelectric force microscopy is usually restricted to studies near the surface of samples, while EFG studies can be performed in bulk or at the surface of materials, by using diffusion, evaporation, or implantation techniques to add the probe atoms in the environments to study.

Therefore we hope this work will stimulate more EFG studies. However, one limitation of our results should be mentioned. In this paper we have analyzed the variation of the EFG with the scaling of the ferroelectric distortions as a whole. However, in experiments, the parameters, such as temperature, in general produce variations involving, for example, additional distortion modes, lattice vibrations, and lattice expansions. The variation of each independent atomic displacement may have a complex variation with changing temperature. Therefore the relation investigated here cannot be directly used to infer polarization variations from EFGs or vice versa, except in well understood cases. Further work to improve this limitation could involve the study of different structural changes or temperature effects.

ACKNOWLEDGMENTS

This work has been supported by the AQUIFER (Aquila Initiative for Ferroics) research program, sponsored by the International Center for Materials Research (ICMR) at UCSB, and research projects PTDC/FIS/105416/2008 and CERN/FP/116320/2010. J. N. Gonçalves acknowledges FCT Grant No. SFRH/BD/42194/2007. The theoretical research at CNR-SPIN has received funding by the European Community's Seventh Framework Programme FP7/2007-2013 under Grant No. 203523-BISMUTH. A.S. thanks P. Barone for comments on the manuscript. Computational support by CASPUR Supercomputing center in Rome is acknowledged.

*joaonsg@ua.pt

[1]D. Khomskii, Physics **2**, 20 (2009).
[2]S.-W. Cheong and M. Mostovoy, Nat. Mater. **6**, 13 (2007).
[3]I. B. Bersuker, Phys. Rev. Lett. **108**, 137202 (2012).
[4]G. Schatz and A. Weidinger, *Nuclear Condensed Matter Physics: Nuclear Methods and Applications* (Wiley, New York, 1996).
[5]*Physics of Ferroelectrics: A Modern Perspective*, edited by K. Rabe, C. H. Ahn, and J.-M. Triscone (Springer, Berlin, 2007).
[6]R. D. King-Smith and D. Vanderbilt, Phys. Rev. B **47**, 1651 (1993).
[7]R. Resta, Rev. Mod. Phys. **66**, 899 (1994).
[8]P. Blaha, K. Schwarz, and P. Herzig, Phys. Rev. Lett. **54**, 1192 (1985).
[9]P. Blaha and K. Schwarz, J. Phys. F **17**, 899 (1987).
[10]P. Blaha, K. Schwarz, and P. H. Dederichs, Phys. Rev. B **37**, 2792 (1988).
[11]P. Blaha and K. Schwarz, Hyperfine Interact. **52**, 153 (1989).
[12]C. Ambrosch-Draxl, P. Blaha, and K. Schwarz, J. Phys.: Condens. Matter **1**, 4491 (1989).
[13]C. Ambrosch-Draxl, P. Blaha, and K. Schwarz, Phys. Rev. B **44**, 5141 (1991).
[14]P. Blaha, D. J. Singh, P. I. Sorantin, and K. Schwarz, Phys. Rev. B **46**, 1321 (1992).
[15]T. Oja and P. A. Casabella, Phys. Rev. **177**, 830 (1969).
[16]M. E. Fitzgerald and P. A. Casabella, Phys. Rev. B **2**, 1350 (1970).

[17]M. E. Fitzgerald and P. A. Casabella, Phys. Rev. B **7**, 2193 (1973).
[18]F. Haarmann, K. Koch, P. Jeglič, H. Rosner, and Y. Grin, Chem. Eur. J. **17**, 7560 (2011).
[19]R. Bjornsson and M. Bühl, Dalton Trans. **39**, 5319 (2010).
[20]S. Jalali Asadabadi, Phys. Rev. B **75**, 205130 (2007).
[21]A. M. L. Lopes, G. N. P. Oliveira, T. M. Mendonça, J. A. Moreira, A. Almeida, J. P. Araújo, V. S. Amaral, and J. G. Correia, Phys. Rev. B **84**, 014434 (2011).
[22]Y. Yeshurun, Solid State Commun. **27**, 181 (1978).
[23]V. Bhide and M. Multani, Phys. Rev. **149**, 289 (1966).
[24]A. M. L. Lopes, J. P. Araújo, V. S. Amaral, J. G. Correia, Y. Tomioka, and Y. Tokura, Phys. Rev. Lett. **100**, 155702 (2008).
[25]D. C. Dening and P. A. Casabella, J. Magn. Reson. **38**, 277 (1980).
[26]Y. Yeshurun, J. Phys. Chem. Solids **40**, 231 (1979).
[27]O. Kanert, H. Schulz, and J. Albers, Solid State Commun. **91**, 465 (1994).
[28]R. D. King-Smith and D. Vanderbilt, Phys. Rev. B **49**, 5828 (1994).
[29]G. H. Kwei, A. C. Lawson, S. J. L. Billinge, and S.-W. Cheong, J. Phys. Chem. **97**, 2368 (1993).
[30]P. E. Blöchl, Phys. Rev. B **50**, 17953 (1994).
[31]G. Kresse and J. Furthmüller, Phys. Rev. B **54**, 11169 (1996).
[32]J. P. Perdew, K. Burke, and M. Ernzerhof, Phys. Rev. Lett. **77**, 3865 (1996).
[33]P. Blaha, K. Schwarz, G. Madsen, D. Kvasnicka, and J. Luitz, *WIEN2k, An Augmented Plane Wave Plus Local Orbitals Program for Calculating Crystal Properties*, Techn. Universität Wien, Vienna, 2001.
[34]A. W. Hewat, J. Phys. C **6**, 1074 (1973).
[35]G. Shirane, R. Newnham, and R. Pepinsky, Phys. Rev. **96**, 581 (1954).
[36]S. A. Mabud, J. Appl. Crystallogr. **12**, 49 (1979).
[37]W. F. Nelmes, Solid State Commun. **54**, 721 (1985).
[38]For $KNbO_3$ and $PbTiO_3$ the same shape of energy curve is obtained with energy differences of 30 and 20 meV and theoretical distortions at 85 and 94%. For the other compounds the energy minimum is the undistorted phase, as expected, except for $LiNbO_3$ which has a minimum at small values of distortion.
[39]R. Resta, M. Posternak, and A. Baldereschi, Phys. Rev. Lett. **70**, 1010 (1993).
[40]H. Wieder, Phys. Rev. **99**, 1161 (1955).
[41]For BaTiO3 and $KNbO_3$ we considered the displacements also in opposite directions, with P taking negative and positive values. In other cases the distortion is taken only for the positive direction along the polar axis. In this case, P is increasing from 0 to a maximum.
[42]K. Koch, R. O. Kuzian, K. Koepernik, I. V. Kondakova, and H. Rosner, Phys. Rev. B **80**, 125113 (2009).
[43]R. E. Alonso, C. O. Rodríguez, and A. López García, Phys. Rev. B **69**, 212106 (2004).
[44]R. Blinc, V. V. Laguta, B. Zalar, M. Itoh, and H. Krakauer, J. Phys.: Condens. Matter **20**, 085204 (2008).
[45]Z. Wu and R. E. Cohen, Phys. Rev. B **73**, 235116 (2006).
[46]J. P. Perdew and Y. Wang, Phys. Rev. B **45**, 13244 (1992).
[47]R. Hewitt, Phys. Rev. **121**, 42 (1961).
[48]N. Stone, At. Data Nucl. Data Tables **90**, 75 (2005).
[49]D. Padro, V. Jennings, M. E. Smith, R. Hoppe, P. A. Thomas, and R. Dupree, J. Phys. Chem. B **106**, 13176 (2002).
[50]G. Czjzek, Hyperfine Interact. **14**, 189 (1983).
[51]T. Butz, M. Ceolín, P. Ganal, P. Schmidt, M. A. Taylor, and W. Tröger, Phys. Scr. **54**, 234 (1996).
[52]T. Butz, Phys. Scr. **82**, 025702 (2010).